PERGAMON

International Journal of Solids and Structures 38 (2001) 1295–1309

INTERNATIONAL JOURNAL OF SOLIDS and STRUCTURES

www.elsevier.com/locate/ijsolstr

Dynamic stability analysis of functionally graded cylindrical shells under periodic axial loading

T.Y. Ng [a], K.Y. Lam [a], K.M. Liew [b,*], J.N. Reddy [c]

[a] *Institute of High Performance Computing, 89C Science Park Drive, #02-11/12, The Rutherford, Singapore Science Park 1, Singapore 118261, Singapore*

[b] *Centre for Advanced Numerical Engineering Simulations, School of Mechanical and Production Engineering, Nanyang Technological University, Nanyang Avenue, Singapore 639798, Singapore*

[c] *Department of Mechanical Engineering, Texas A & M University, College Station, TX 77843-3123, USA*

Received 12 April 1999; in revised form 3 March 2000

Abstract

In this paper, a formulation for the dynamic stability analysis of functionally graded shells under harmonic axial loading is presented. A profile for the volume fraction is assumed and a normal-mode expansion of the equations of motion yields a system of Mathieu–Hill equations the stability of which is analyzed by the Bolotin's method. The present study examines the effects of the volume fraction of the material constituents and their distribution on the parametric response, in particular the positions and sizes of the instability regions.

Keywords: Dynamic stability; Parametric resonance; Functionally graded; Cylindrical shell

1. Introduction

The use of functionally graded materials has gained much popularity in recent years especially in extreme high temperature environments. Functionally graded materials are composite materials, which are microscopically inhomogeneous, and the mechanical properties vary smoothly or continuously from one surface to the other. It is this continuous change that results in gradient properties in functionally graded materials. Typically, these materials are made from a mixture of ceramic and metal, or a combination of different metals. Unlike fiber-matrix composites which have a mismatch of mechanical properties across an interface of two discrete materials bonded together and may result in debonding at high temperatures, functionally graded materials have the advantage of being able to withstand high temperature gradient environments while maintaining their structural integrity. The ceramic material provides high temperature

* Corresponding author. Tel.: +65-790-4076; fax: +65-791-1859.
E-mail address: mkmliew@ntu.edu.sg (K.M. Liew).

0020-7683/01/$ - see front matter
PII: S0020-7683(00)00090-1

Nomenclature

A_{ij}, B_{ij}, D_{ij} extensional, coupling, bending stiffnesses
A_{mnj}, B_{mnj}, C_{mnj} modal constants
e_x, e_θ normal strain components
$e_{x\theta}$ shear strain component
e_1, e_2, μ reference surface strains
k_1, k_2, τ reference surface curvatures
E elastic modulus
h shell thickness
L shell length
m axial half wave number
n circumferential wave number
λ_m $m\pi/L$
M_x, M_θ, $M_{x\theta}$ moment resultants
N_x, N_θ, $N_{x\theta}$ force resultants
M_{IJ}, K_{IJ}, Q_{IJ} characteristic matrices of Mathieu–Hill's equation
N_a pulsating axial load
N_0 static component of N_a
N_s harmonic component of N_a
N_{cr} static buckling load
P excitation frequency
p nondimensionalized P
q_{mnj} generalized coordinate
R shell radius
T time
u, v, w orthogonal components of displacement field
V volume fraction
Φ power law exponent
x, θ, z shell coordinates
ρ mass density
ρ_t mass density per unit length
ν Poisson's ratio
ω shell natural frequency
Θ angle subtended by unstable region

resistance due to its low thermal conductivity while the ductile metal component prevents fracture due to thermal stresses.

Functionally graded materials are now being strongly considered as a potential structural material for future high-speed spacecraft. They are also developed now for the general use as structural components in high temperature environments. Many studies have examined functionally graded materials as thermal barriers. With the increased usage of these materials, it is also important to understand the dynamics of functionally graded material structures. A few studies have addressed this. The elastic problem of thick-walled tubes of a functionally graded material under internal pressure in the case of plane strain has been studied (Fukui and Yamanaka, 1992). Rooney and Ferrari (1994) presented the solution to the problem of

torsion of an inhomogeneous functionally graded shaft with rectangular cross-section where a methodology was developed to reduce the problem to the solution of a simple linear ordinary differential equation. A formulation of the stability problem for functionally graded hybrid composite plates was presented by Birman (1995) where a micromechanical model was employed to solve the buckling problem for a rectangular plate subjected to uniaxial compression. The correlation between hardness and residual stress in layered functionally graded materials was examined by Omori et al. (1995). It was found that the functionally graded materials considered exhibited two kinds of residual stresses, a local stress which is stored in each layer, and a layer stress is dispersed throughout each layer of the whole material. Durodola and Adlington (1996) presented the use of numerical methods to assess the effect of various forms of gradation of material properties to control deformation and stresses in rotating axisymmetric components such as disks and rotors.

Studies of buckling of thin-walled isotropic cylinders under axial compression, torsional loadings, bending, hydrostatic pressure and lateral pressure have been extensively covered in the literature. However, structural components under periodic loads can undergo parametric resonance which may occur over a range of forcing frequencies and if the load is compressive to the structure, resonance or instability can and usually occurs even if the magnitude of the load is below the critical buckling load of the structure. It is thus, of prime importance to investigate the dynamic stability of dynamic systems under periodic loads. The parametric resonance of the cylindrical shells under axial loads has become a popular subject of study. It was first examined by Bolotin (1964), Yao (1965) and Vijayaraghavan and Evan-Iwanowski (1967). For thin cylindrical shells under periodic axial loads, the method of solution is almost always to first reduce the equations of motion to a system of Mathieu–Hill equations. The dynamic stability for such a system of equations can then be analyzed by a number of methods.

In this paper, the parametric resonance or dynamic stability of functionally graded cylindrical shells under periodic axial loading is studied using Bolotin's first approximation. This work is a natural extension of a previous piece of work by the present authors (Lam and Ng, 1997) on the dynamic stability of isotropic cylindrical shells. This piece of work was motivated by the increased general use of functionally graded materials and also a need to understand their dynamic responses.

2. Theory and formulation

The functionally graded cylindrical shell as shown in Fig. 1 is assumed to be thin and of length L, thickness h and radius R. The x-axis is taken along a generator, the circumferential arc length subtends an angle θ, and the z-axis is directed radially inwards. The periodic extensional axial load per unit length is given by

$$N_a = N_0 + N_s \cos Pt, \tag{1}$$

where P is the frequency of excitation in radians per unit time. The equations of motion according to Donnell's theory are thus given by

$$\frac{\partial N_x}{\partial x} + \frac{1}{R}\frac{\partial N_{x\theta}}{\partial \theta} = \rho_t \frac{\partial^2 u}{\partial t^2}, \tag{2}$$

$$\frac{\partial N_{x\theta}}{\partial x} + \frac{1}{R}\frac{\partial N_{\theta}}{\partial \theta} = \rho_t \frac{\partial^2 v}{\partial t^2}, \tag{3}$$

$$\frac{\partial^2 M_x}{\partial x^2} + \frac{2}{R}\frac{\partial^2 M_{x\theta}}{\partial x \partial \theta} + \frac{1}{R^2}\frac{\partial^2 M_{\theta}}{\partial \theta^2} - \frac{1}{R}N_{\theta} + \frac{\partial}{\partial x}\left(N_a \frac{\partial w}{\partial x}\right) = \rho_t \frac{\partial^2 w}{\partial t^2}, \tag{4}$$

where u, v and w are the components of displacement for an element of the shell wall, and

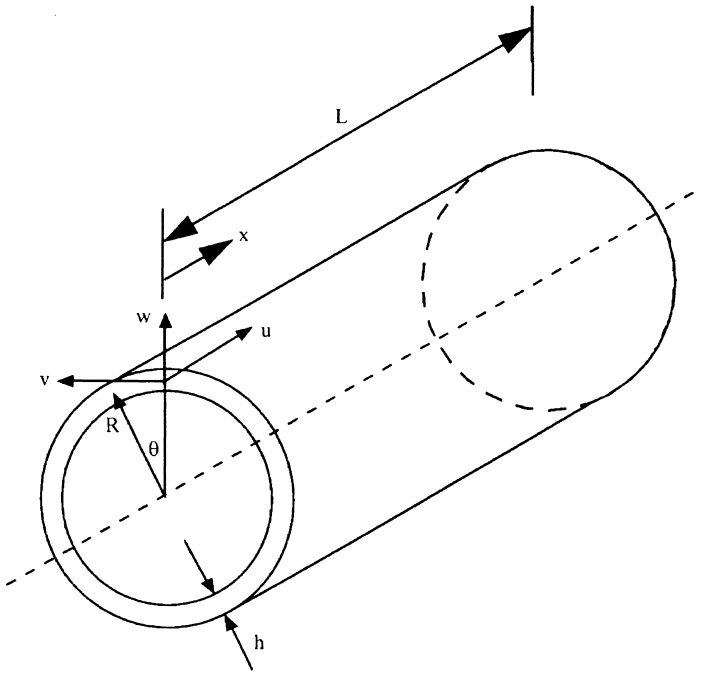

Fig. 1. Coordinate system of the FGM cylindrical shell.

$$\rho_t = \int_{-h/2}^{h/2} \rho(z)\,\mathrm{d}z. \tag{5}$$

The stress and moment resultants are defined as

$$\begin{Bmatrix} N_x \\ N_\theta \\ N_{x\theta} \\ M_x \\ M_\theta \\ M_{x\theta} \end{Bmatrix} = \begin{bmatrix} A_{11} & A_{12} & A_{16} & B_{11} & B_{12} & B_{16} \\ A_{12} & A_{22} & A_{26} & B_{12} & B_{22} & B_{26} \\ A_{16} & A_{26} & A_{66} & B_{16} & B_{26} & B_{66} \\ B_{11} & B_{12} & B_{16} & D_{11} & D_{12} & D_{16} \\ B_{12} & B_{22} & B_{26} & D_{12} & D_{22} & D_{26} \\ B_{16} & B_{26} & B_{66} & D_{16} & D_{26} & D_{66} \end{bmatrix} \begin{Bmatrix} e_1 \\ e_2 \\ \gamma \\ k_1 \\ k_2 \\ \tau \end{Bmatrix}, \tag{6}$$

where

$$\left(A_{ij}, B_{ij}, D_{ij}\right) = \int_{-h/2}^{h/2} Q_{ij}\left(1, z, z^2\right)\mathrm{d}z \quad (i,j = 1,2,6), \tag{7}$$

and

$$Q_{11} = Q_{22} = \frac{E_{\mathrm{eff}}}{1 - v_{\mathrm{eff}}^2}, \tag{8}$$

$$Q_{12} = v_{\mathrm{eff}} \frac{E_{\mathrm{eff}}}{1 - v_{\mathrm{eff}}^2}, \tag{9}$$

$$Q_{66} = \frac{E_{\mathrm{eff}}}{2(1 + v_{\mathrm{eff}})}, \tag{10}$$

$$Q_{16} = Q_{26} = 0, \tag{11}$$

where E_{eff} and v_{eff} are the effective elastic modulus and effective Poisson's ratio of the functionally graded shell, respectively, and will be defined subsequently.

The strain components e_x, e_θ and $e_{x\theta}$ which are the strains in the x direction, the circumferential direction and the shear strain in the $x\theta$-plane of the middle surface, respectively, can be expressed as

$$e_x = e_1 + zk_1, \tag{12}$$

$$e_\theta = e_2 + zk_2, \tag{13}$$

$$e_{x\theta} = \gamma + z\tau. \tag{14}$$

The strain and curvatures are defined by Donnell's theory as

$$e_1 = \frac{\partial u}{\partial x}, \tag{15}$$

$$e_2 = \frac{1}{R}\left(\frac{\partial v}{\partial \theta} + w\right), \tag{16}$$

$$\gamma = \frac{\partial v}{\partial x} + \frac{1}{R}\frac{\partial u}{\partial \theta}, \tag{17}$$

$$k_1 = -\frac{\partial^2 w}{\partial x^2}, \tag{18}$$

$$k_2 = -\frac{1}{R^2}\frac{\partial^2 w}{\partial \theta^2}, \tag{19}$$

$$\tau = -\frac{2}{R}\frac{\partial^2 w}{\partial x\,\partial \theta}. \tag{20}$$

In order to accurately model the material properties of functionally graded materials, the properties must be both temperature dependent and position dependent. This is achieved by using a simple rule of mixtures for the stiffness parameters coupled with the temperature dependent properties of the constituents. The volume fraction is a spatial function and the properties of the constituents are functions of the temperature. The combination of these functions give rise to the effective material properties of functionally graded materials and can be expressed as

$$F_{\text{eff}}(T,z) = F_{\text{c}}(T)V(z) + F_{\text{m}}(T)(1 - V(z)), \tag{21}$$

where F_{eff} is the effective material property of the functionally graded material, F_{c} and F_{m} are the temperature dependent properties of the ceramic and metal respectively, and V is the volume fraction of the ceramic constituent of the functionally graded material. In addition, a simple power law exponent of the volume fraction distribution is used to provide a measure of the amount of ceramic and metal in the functionally graded material. In the present case, the volume fraction is defined as

$$V(z) = \left(\frac{z + h/2}{h}\right)^{\Phi}, \tag{22}$$

where Φ is the power law exponent $(0 \leqslant \Phi \leqslant \infty)$.

According to the above distribution described in Eq. (21), the inner surface of the cylindrical shell is metal rich and the outer surface is ceramic rich. We shall name this type of material as Type A. For a

cylindrical shell that is ceramic rich at the inner surface and metal rich at the outer surface which we shall name Type B, the effective material properties are expressed as

$$F_{\text{eff}}(T,z) = F_{\text{m}}(T)V(z) + F_{\text{c}}(T)(1 - V(z)). \tag{23}$$

Assuming the shell to be simply supported, there exists a solution for the equations of motion in the form

$$u_{mn} = A_{mn}\mathrm{e}^{\mathrm{i}\omega t}\cos\lambda_m x\cos n\theta, \tag{24}$$

$$v_{mn} = B_{mn}\mathrm{e}^{\mathrm{i}\omega t}\sin\lambda_m x\sin n\theta, \tag{25}$$

$$w_{mn} = C_{mn}\mathrm{e}^{\mathrm{i}\omega t}\sin\lambda_m x\cos n\theta, \tag{26}$$

where n represents the number of circumferential waves, m, the number of axial half waves in the corresponding standing wave pattern and $\lambda_m = m\pi/L$. ω represents the natural frequency of the cylindrical shell under constant axial loading N_0.

The equations of motion can be solved using an eigenfunction expansion of the normal modes of free vibration of a cylindrical shell under a constant axial load N_0 with the oscillating component $N_s = 0$. Substitution of the above three equations into the equations of motion which are also a set of three coupled homogeneous equations yields a cubic frequency equation when the determinant is equated to zero.

$$\begin{bmatrix} C_{11} & C_{12} & C_{13} \\ C_{21} & C_{22} & C_{23} \\ C_{31} & C_{32} & C_{33} \end{bmatrix} \begin{Bmatrix} A_{mn} \\ B_{mn} \\ C_{mn} \end{Bmatrix} = \begin{Bmatrix} 0 \\ 0 \\ 0 \end{Bmatrix}, \tag{27}$$

where the C_{ij}'s are defined in the appendix. Thus, for each m and n, there exists three roots corresponding to the transverse, axial and circumferential modes.

To solve the equations of motion that include the oscillating component N_s, a solution is sought in the form shown below where all the modes are superimposed.

$$u_{mnj} = \sum_{j=1}^{3}\sum_{m=1}^{\infty}\sum_{n=1}^{\infty} A_{mnj}q_{mnj}(t)\cos\lambda_m x\cos n\theta, \tag{28}$$

$$v_{mnj} = \sum_{j=1}^{3}\sum_{m=1}^{\infty}\sum_{n=1}^{\infty} B_{mnj}q_{mnj}(t)\sin\lambda_m x\sin n\theta, \tag{29}$$

$$w_{mnj} = \sum_{j=1}^{3}\sum_{m=1}^{\infty}\sum_{n=1}^{\infty} C_{mnj}q_{mnj}(t)\sin\lambda_m x\cos n\theta, \tag{30}$$

where $q_{mnj}(t)$ is a generalized coordinate.

Substituting the above three equations into the equations of motion and simplifying yields

$$\sum_{j=1}^{3}\sum_{m=1}^{\infty}\sum_{n=1}^{\infty}\left(\ddot{q}_{mnj} + \omega_{mnj}^2 q_{mnj}\right)\alpha_{mnj}\cos\lambda_m x\cos n\theta = 0, \tag{31}$$

$$\sum_{j=1}^{3}\sum_{m=1}^{\infty}\sum_{n=1}^{\infty}\left(\ddot{q}_{mnj} + \omega_{mnj}^2 q_{mnj}\right)\beta_{mnj}\sin\lambda_m x\sin n\theta = 0, \tag{32}$$

$$\sum_{j=1}^{3}\sum_{m=1}^{\infty}\sum_{n=1}^{\infty}\left(\ddot{q}_{mnj} + \omega_{mnj}^2 q_{mnj}\right)\sin\lambda_m x\cos n\theta - \frac{1}{\rho_{\text{t}}}\lambda_m\cos Pt\sum_{j=1}^{3}\sum_{m=1}^{\infty}\sum_{n=1}^{\infty} q_{mnj}\frac{\partial}{\partial x}(N_s\cos\lambda_m x)\cos n\theta = 0, \tag{33}$$

where

$$\alpha_{mnj} = \frac{A_{mnj}}{C_{mnj}}, \qquad \beta_{mnj} = \frac{B_{mnj}}{C_{mnj}}. \tag{34}$$

Making use of the orthogonality condition, we multiply Eq. (31) by $\alpha_{rsi}\cos\lambda_r x \sin s\theta$, Eq. (32) by $\beta_{rsi}\sin\lambda_r x \sin s\theta$, and Eq. (33) by $\sin\lambda_r x \cos s\theta$. This yields a set of equations

$$M_{IJ}\ddot{q}_J + (K_{IJ} - \cos Pt Q_{IJ})q_J = 0, \tag{35}$$

where M_{IJ}, K_{IJ} and Q_{IJ} are matrices and $\ddot{q}_J$ and q_J are column vectors consisting of the $\ddot{q}_{mnj}$'s and q_{mnj}'s, respectively. The subscripts r, s, i, m, n, j, I and J have the following ranges:

$$\begin{aligned} &r, s, m, n = 1, 2, 3, 4, \ldots, N, \\ &i, j = 1, 2, 3, \\ &I, J = 1, 2, 3, 4, \ldots, (N \times N \times 3). \end{aligned} \tag{36}$$

The matrices M_{IJ}, K_{IJ} and Q_{IJ} are given as

$$\begin{aligned} M_{IJ} &= \int_0^L \int_0^{2\pi} (\alpha_I \alpha_J \cos\lambda_r x \cos s\theta \cos\lambda_m x \cos n\theta + \beta_I \beta_J \sin\lambda_r x \sin s\theta \sin\lambda_m x \sin n\theta \\ &\quad + \sin\lambda_r x \cos s\theta \sin\lambda_m x \cos n\theta) \mathrm{d}\theta \, \mathrm{d}x \\ &= \begin{cases} \pi L/2(1 + \beta_I\beta_J + \alpha_I\alpha_J) & \text{if } I = J, \\ 0 & \text{if } I \neq J. \end{cases} \end{aligned} \tag{37}$$

$$K_{IJ} = \omega_J^2 M_{IJ}, \tag{38}$$

$$\begin{aligned} Q_{IJ} &= \frac{1}{\rho_t}\lambda_m \int_0^L \int_0^{2\pi} \frac{\partial}{\partial x}(N_s \cos\lambda_m x \cos n\theta) \sin\lambda_r x \cos s\theta \mathrm{d}\theta \mathrm{d}x \\ &= \begin{cases} -\pi L/(2\rho_t)\lambda_r\lambda_m N_s & \text{if } I = J, \\ 0 & \text{if } I \neq J. \end{cases} \end{aligned} \tag{39}$$

3. Stability analysis

Eq. (35) is in the form of a second order differential equation with periodic coefficients of the Mathieu–Hill type. The regions of unstable solutions are separated by periodic solutions having period T and $2T$ with $T = 2\pi/P$. The solutions with period $2T$ are of greater practical importance as the widths of these unstable regions are usually larger than those associated with solutions having period T. Using Bolotin's (1964) first approximation, the periodic solutions with period $2T$ can be sought in the form

$$f = a\sin\frac{Pt}{2} + b\cos\frac{Pt}{2}, \tag{40}$$

where a and b are arbitrary vectors.

Substituting Eq. (40) into Eq. (35) and equating the coefficients of the $\sin(Pt/2)$ and $\cos(Pt/2)$ terms, a set of linear homogeneous algebraic equations in terms of a and b can be obtained. The conditions for nontrivial solutions are given by

$$\det\begin{bmatrix} K_{IJ} - \frac{1}{2}Q_{IJ} - \frac{1}{4}P^2 M_{IJ} & 0 \\ 0 & K_{IJ} + \frac{1}{2}Q_{IJ} - \frac{1}{4}P^2 M_{IJ} \end{bmatrix} = 0. \tag{41}$$

Instead of solving the above nonlinear geometric equations for P, the above equation can be rearranged to the standard form of a generalized eigenvalue problem

$$\det\left[\begin{pmatrix} K_{IJ}-\frac{1}{2}Q_{IJ} & 0 \\ 0 & K_{IJ}+\frac{1}{2}Q_{IJ}\end{pmatrix}-P^2\begin{pmatrix}\frac{1}{4}M_{IJ} & 0 \\ 0 & \frac{1}{2}M_{IJ}\end{pmatrix}\right]=0, \tag{42}$$

where 0 is a $N\times N$ null matrix.

4. Numerical results and discussion

The ceramic material used in this study is silicon nitride and the metal material used is nickel. The densities and Poisson's ratios of the materials are in this case independent of the temperature. The density of silicon nitride is taken to be 2370 kg/m^3 and that of nickel is 8900 kg/m^3. The Poisson's ratio is 0.24 for silicon nitride and 0.31 for nickel. The elastic moduli are however, temperature dependent and are obtained from Touloukian (1967) as

$$E_{\rm sn}=348.43\times10^9\left(1-3.070\times10^{-4}\ T+2.160\times10^{-7}\ T^2-8.946\times10^{-11}\ T^3\right), \tag{43}$$

$$E_{\rm ni}=223.95\times10^9\left(1-2.794\times10^{-4}\ T-3.998\times10^{-9}\ T^2\right), \tag{44}$$

where $E_{\rm sn}$ and $E_{\rm ni}$ are the elastic moduli of silicon nitride and nickel, respectively, and T is the temperature in Kelvin. The nondimensional excitation frequency parameter p for the FGM shell is defined as

$$p=2\pi Rp\left(\frac{\rho_{\rm t}}{A_{11}}\right)^{1/2}. \tag{45}$$

Each unstable region is bounded by two lines which originate from a common point from the p-axis. The two curves appear at the first glance to be straight lines but are in fact, two very slight "outward" curving plots. For the sake of tabular presentation, each unstable region is defined by its point of origin from the p-axis with $N_s=0$. The angle subtended, Θ, is also introduced to give a measure of the size of the unstable region. It is calculated based on the arctangent of the right-angled triangle, abc, as shown in Fig. 2. This angle gives an accurate measure of the slope of the boundary of the unstable region as calculations done with the smaller similar triangle, ab$'$c$'$ (Fig. 2), are within 0.1%.

The values of N_0 are chosen to be in terms of $N_{\rm cr}$ which is the critical buckling load of a simply supported circular cylindrical shell subjected to static compressive axial load. From Timoshenko and Gere (1961), this is conservatively chosen to be in terms of the nickel material and is thus given as

$$N_{\rm cr}=\frac{E_{\rm ni}h^2}{R\left[3\left(1-v_{\rm ni}^2\right)\right]^{1/2}}. \tag{46}$$

Fig. 3 gives an illustrative graphical representation of Table 1 which are the results for mode (1,1) of a Type A shell under tensile loading of $N_0=0.5N_{\rm cr}$. Results for mode (1,1) of a Type B shell under similar loading are given in Table 2. The results for mode (1,1) of a Type A shell under compressive loading of $N_0=-0.5N_{\rm cr}$ are given in Table 3. For a Type B shell under similar compressive loading, results are presented in Table 4. Corresponding results for mode (1,2) are given in Tables 5–8. An initial study has been conducted to show the effects of the geometric parameters, L/R and R/h, on the unstable regions of a simply supported isotropic cylindrical shell. The results are presented in Figs. 4 and 5. It is observed that

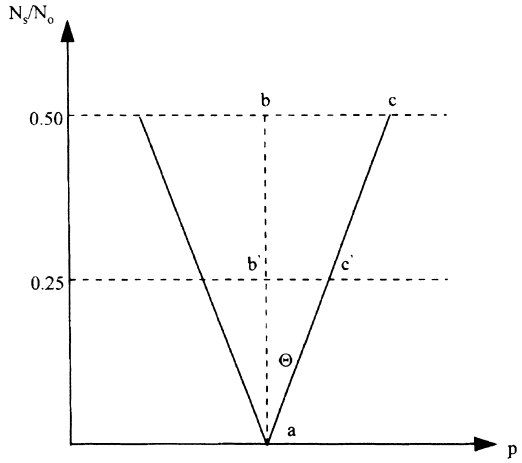

Fig. 2. An unstable region in the N_s/N_0-p plane.

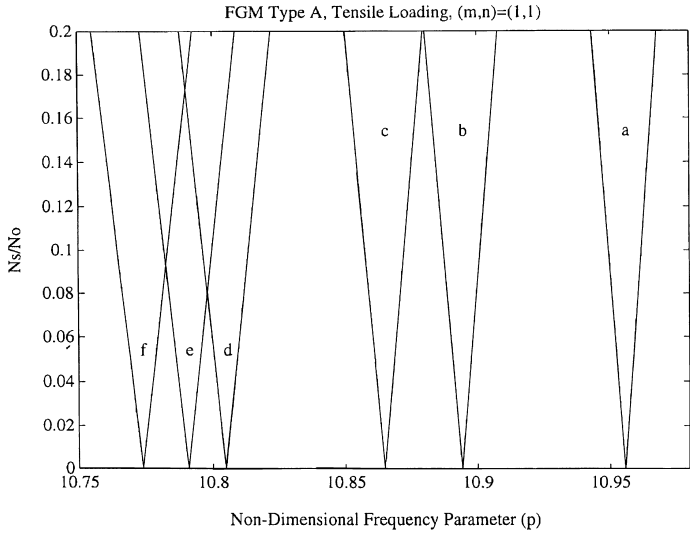

Fig. 3. Unstable regions for the transverse mode of mode (1,1) of a simply supported silicon nitride-nickel FGM Type A cylindrical shell of geometric properties $L/R = 1$ and $R/h = 100$ and subjected to extensional loading of $N_0 = 0.5N_{cr}$ (a) $\Phi = 0$, (b) $\Phi = 0.5$, (c) $\Phi = 1$, (d) $\Phi = 5$, (e) $\Phi = 10$, (f) $\Phi = \infty$.

with a decrease in length or an increase in thickness, i.e. overall increase in stiffness, the unstable regions shift to the right having higher points of origins. A detailed discussion on this can be found in Lam and Ng (1997).

The dynamic stability results for the FGM shell presented in Tables 1–8 are for a simply supported silicon nitride–nickel FGM cylindrical shell of geometric properties $L/R = 1$ and $R/h = 100$ for both Type A and Type B materials. The results present the transverse modes only and the two higher axial and circumferential modes are not shown. Results presented are for different values of the power law exponent Φ for the transverse modes of $(m, n) = (1, 1), (1, 2)$. The results presented are for $\Phi = 0, 0.5, 1, 5, 10, \infty$. For

Table 1
Unstable regions for the transverse mode of mode (1,1) of a simply supported silicon nitride–nickel FGM Type A cylindrical shell of geometric properties $L/R = 1$ and $R/h = 100$ and subjected to extensional loading of $N_0 = 0.5N_{cr}$

Φ	Point of origin p	Θ ($\times 10^{-2}$)
0	10.955605	6.12220
0.5	10.894118	6.90880
1	10.864882	7.38560
5	10.804910	8.57300
10	10.790882	8.89840
∞	10.773959	9.32320

Table 2
Unstable regions for the transverse mode of mode (1,1) of a simply supported silicon nitride–nickel FGM Type B cylindrical shell of geometric properties $L/R = 1$ and $R/h = 100$ and subjected to extensional loading of $N_0 = 0.5N_{cr}$

Φ	Point of origin p	Θ ($\times 10^{-2}$)
0	10.773959	9.32320
0.5	10.848743	7.92440
1	10.882963	7.37660
5	10.936770	6.48780
10	10.946016	6.31620
∞	10.946016	6.12220

Table 3
Unstable regions for the transverse mode of mode (1,1) of a simply supported silicon nitride–nickel FGM Type A cylindrical shell of geometric properties $L/R = 1$ and $R/h = 100$ and subjected to compressive loading of $N_0 = -0.5N_{cr}$

Φ	Point of origin p	Θ ($\times 10^{-2}$)
0	10.707442	6.26980
0.5	10.613564	7.09860
1	10.564626	7.60400
5	10.455408	8.87120
10	10.427831	9.22080
∞	10.427831	9.67880

Table 4
Unstable regions for the transverse mode of mode (1,1) of a simply supported silicon nitride–nickel FGM Type B cylindrical shell of geometric properties $L/R = 1$ and $R/h = 100$ and subjected to compressive loading of $N_0 = -0.5N_{cr}$

Φ	Point of origin p	Θ ($\times 10^{-2}$)
0	10.393196	9.67880
0.5	10.526190	8.17680
1	10.583092	7.59400
5	10.673575	6.65400
10	10.689887	6.47320
∞	10.707442	6.26980

Type A material, when $\Phi = 0$, the shell is fully ceramic (silicon nitrate) and when $\Phi = \infty$, the shell is fully metal (nickel). For Type B material, the converse is true. Due to its higher elastic modulus, the sizes of the unstable regions associated with the ceramic material $\Phi = 0$ are 50–55% smaller than those for the metal

Table 5
Unstable regions for the transverse mode of mode (1,2) of a simply supported silicon nitride–nickel FGM Type A cylindrical shell of geometric properties $L/R = 1$ and $R/h = 100$ and subjected to extensional loading of $N_0 = 0.5N_{cr}$

Φ	Point of origin p	Θ ($\times 10^{-2}$)
0	8.5194084	7.64278
0.5	8.4772803	8.62034
1	8.4590579	9.21146
5	8.4268843	10.6771
10	8.4207292	11.0772
∞	8.4141701	11.5984

Table 6
Unstable regions for the transverse mode of mode (1,2) of a simply supported silicon nitride–nickel FGM Type B cylindrical shell of geometric properties $L/R = 1$ and $R/h = 100$ and subjected to extensional loading of $N_0 = 0.5N_{cr}$

Φ	Point of origin p	Θ ($\times 10^{-2}$)
0	8.4141701	11.5984
0.5	8.4601729	9.87008
1	8.4810885	9.19282
5	8.5111333	8.09416
10	8.5154656	7.88210
∞	8.5194084	7.64278

Table 7
Unstable regions for the transverse mode of mode (1,2) of a simply supported silicon nitride–nickel FGM Type A cylindrical shell of geometric properties $L/R = 1$ and $R/h = 100$ and subjected to compressive loading of $N_0 = -0.5N_{cr}$

Φ	Point of origin p	Θ ($\times 10^{-2}$)
0	8.2071402	7.93984
0.5	8.1240355	9.00322
1	8.0809188	9.65170
5	7.9866327	11.2781
10	7.9634231	11.7267
∞	7.9345878	12.3141

Table 8
Unstable regions for the transverse mode of mode (1,2) of a simply supported silicon nitride–nickel FGM Type B cylindrical shell of geometric properties $L/R = 1$ and $R/h = 100$ and subjected to compressive loading of $N_0 = -0.5N_{cr}$

Φ	Point of origin p	Θ ($\times 10^{-2}$)
0	7.9345878	12.3141
0.5	8.0542139	10.3782
1	8.1037601	9.63006
5	8.1799865	8.42888
10	8.1931948	8.19880
∞	8.2071402	7.93984

material $\Phi = \infty$. It is also observed that for all the different values of Φ considered, the regions associated with compressive loadings are generally slightly larger than the corresponding regions associated with

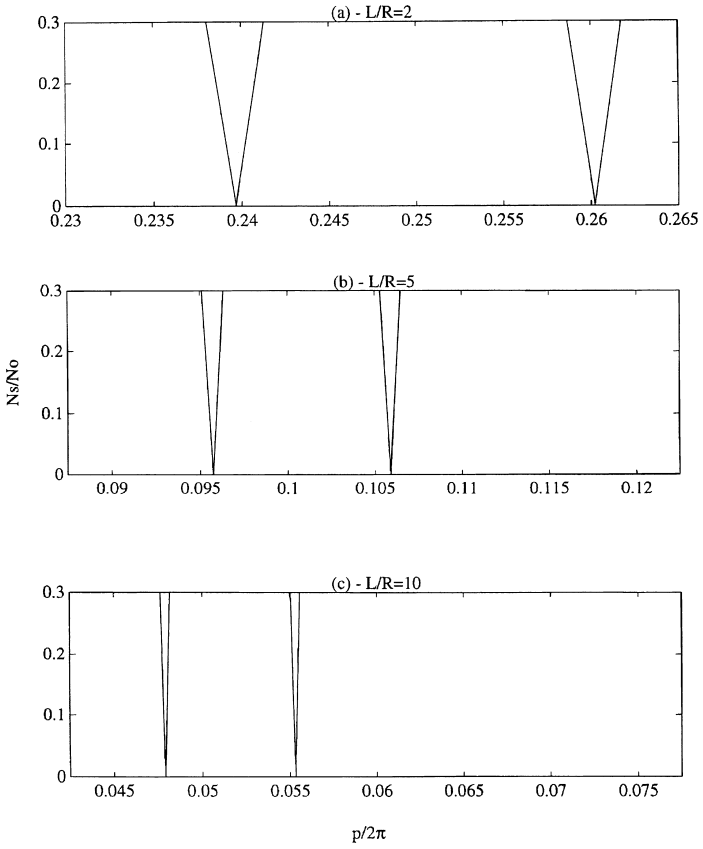

Fig. 4. Variation of the first two unstable regions with shell length for a simply supported isotropic cylindrical shell of thickness ratio $R/h = 100$ and under tensile loading of $N_0 = 0.1N_s$.

tensile loadings. This is consistent with the results reported by Lam and Ng (1997) for the dynamic stability analysis of isotropic cylindrical shells.

From Tables 1–8, it can be observed that as Φ increases from 0 to ∞, the sizes of the unstable regions gradually change from the size associated with $\Phi = 0$ to the size associated with $\Phi = \infty$. It is also observed that at $\Phi = 10$, the results are already very close to those associated with $\Phi = \infty$. Thus, the range of Φ where the results are more sensitive to variation in Φ is about $5 < \Phi < 0$. Traditionally, FGMs were designed as thermal barrier materials for aerospace structures and fusion reactors. However, FGMs are now developed for general use as structural elements in extreme high temperature environments. With the advent and wider use of FGMs, it is important to understand the vibration and dynamic stability behaviors of FGM-material structures.

From this study, it is clear that the natural frequencies – which correspond to half of the value of the point of origin of the unstable regions – and the instability regions can be adjusted according to the material distribution. This is illustrated in Fig. 6, where the variation of the point of origin and unstable region size with the volume exponent is shown. It shows that the unstable region size is much more sensitive to changes in the volume fraction exponent than the point of origin. Thus, by varying the volume fraction of the material constituents in FGM cylindrical shells, the sizes of the unstable regions can be very effectively adjusted or controlled.

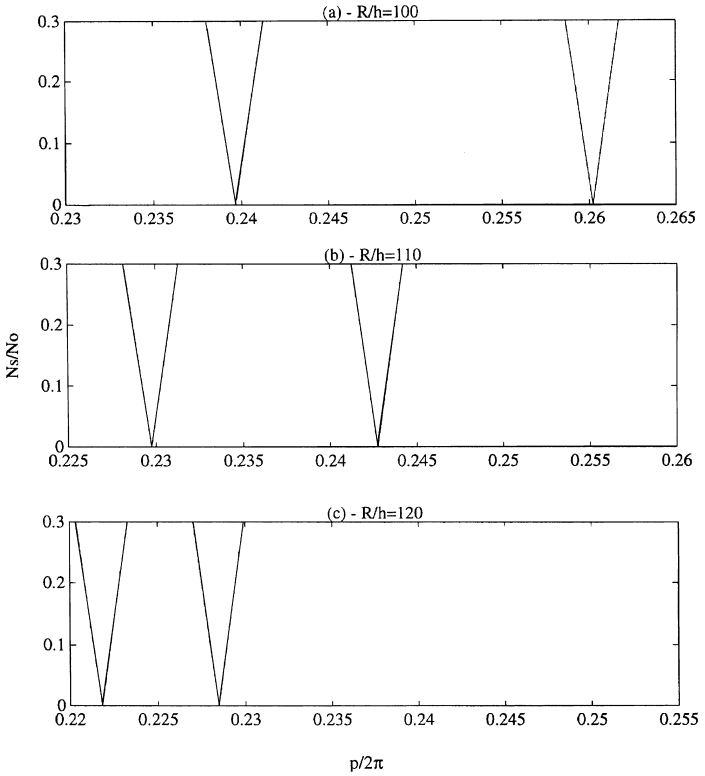

Fig. 5. Variation of the first two unstable regions with shell thickness for a simply supported isotropic cylindrical shell of length ratio $L/R = 2$ and under tensile loading of $N_0 = 0.1N_s$.

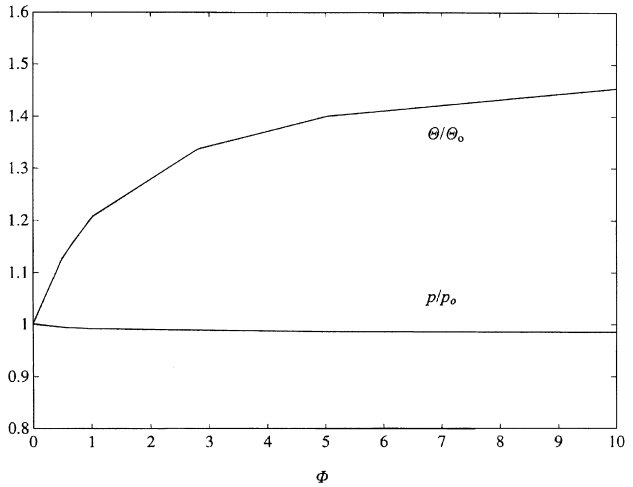

Fig. 6. Variation of the point of origin p and unstable region size Θ with the volume fraction exponent Φ of a simply supported silicon nitride–nickel FGM Type A cylindrical shell of geometric properties $L/R = 1$ and $R/h = 100$ and subjected to extensional loading of $N_0 = 0.5N_{cr}$. p_0 and Θ_0 are the point of origin and unstable region size respectively when $\Phi = 0$.

5. Conclusions

The dynamic stability of simply-supported cylindrical shells of functionally graded material under combined static and periodic axial forces was investigated. Results were found to vary significantly when material distribution was varied by changing the values of the power law exponent which controls the volume fraction of the different materials in the FGM shell. It was also found that reasonable control can be achieved on the natural frequencies and dynamic instability regions by correctly varying the power law exponent.

Appendix A

$$
\begin{aligned}
C_{11} &= A_{11}\lambda_m^2 + \frac{1}{R^2}A_{66}n^2 - \rho_t\omega^2,\\
C_{12} &= -\frac{1}{R}A_{12}\lambda_m n - \frac{1}{R}A_{66}\lambda_m n,\\
C_{13} &= -\frac{1}{R}A_{12}\lambda_m - B_{11}\lambda_m^3 - \frac{1}{R^2}B_{12}\lambda_m n^2 - \frac{2}{R^2}B_{66}\lambda_m n^2,\\
C_{21} &= -\frac{1}{R}A_{12}\lambda_m n - \frac{1}{R}A_{66}\lambda_m n,\\
C_{22} &= A_{66}\lambda_m^2 + \frac{1}{R^2}A_{22}n^2 - \rho_t\omega^2,\\
C_{23} &= \frac{2}{R}B_{66}\lambda_m^2 n + \frac{1}{R^2}A_{22}n + \frac{1}{R}B_{12}\lambda_m^2 n + \frac{1}{R^3}B_{22}n^3,\\
C_{31} &= -\frac{1}{R}A_{12}\lambda_m - B_{11}\lambda_m^3 - \frac{1}{R^2}B_{12}\lambda_m n^2 - \frac{2}{R^2}B_{66}\lambda_m n^2,\\
C_{32} &= \frac{2}{R}B_{66}\lambda_m^2 n + \frac{1}{R^2}A_{22}n + \frac{1}{R}B_{12}\lambda_m^2 n + \frac{1}{R^3}B_{22}n^3,\\
C_{33} &= \frac{2}{R}B_{12}\lambda_m^2 + \frac{2}{R^3}B_{22}n^2 + D_{11}\lambda_m^4 + \frac{1}{R^2}D_{12}(\lambda_m n)^2 + \frac{4}{R^2}D_{66}(\lambda_m n)^2 + \frac{1}{R^2}D_{12}(\lambda_m n)^2 + \frac{1}{R^4}A_{22}\\
&\quad + N_0\lambda_m^2 - \rho_t\omega^2.
\end{aligned}
\tag{A.1}
$$

References

Birman, V., 1995. Buckling of functionally graded hybrid composite plates. Proceedings of the 10th Conference on Engineering Mechanics, Boulder, USA.

Bolotin, V.V., 1964. The Dynamic Stability of Elastic Systems. Holden-Day, San Francisco.

Durodola, J.F., Adlington, J.E., 1996. Functionally graded material properties for disks and rotors. Proceedings of the 1996 First International Conference on Ceramic and Metal Matrix Composites, San Sebastian, Spain.

Fukui, Y., Yamanaka, N., 1992. Elastic analysis for thick-walled tubes of functionally graded material subjected to internal pressure. JSME International Journal, Series 1: Solid Mechanics, Strength of Materials 35, 379.

Lam, K.Y., Ng, T.Y., 1997. Dynamic stability of cylindrical shells subjected to conservative periodic axial loads using different shell theories. Journal of Sound and Vibration 207, 497.

Omori, M., Sakai, H., Nishiyama, K., Suzuki, E., Hirai, T., 1995. Correlation between hardness and residual stress in ZrO//2(3Y)/ metal functionally graded materials. Journal of the Japan Society of Powder and Powder Metallurgy 42, 1384.

Rooney, F.J., Ferrari, M., 1994. Torsion of a functionally graded shaft with rectangular cross-section. Proceedings of the Energy-Sources Technology Conference, New Orleans, USA.

Timoshenko, S.P., Gere, J.M., 1961. Theory of Elasticity. McGraw-Hill, New York.

Touloukian, Y.S., 1967. Thermophysical Properties of High Temperature Solid Materials. Mcmillian, New York.
Vijayaraghavan, A., Evan-Iwanowski, R.M., 1967. Parametric instability of circular cylindrical shells. Journal of Applied Mechanics 31, 985.
Yao, J.C., 1965. Nonlinear elastic buckling and parametric excitation of a cylinder under axial loads. Journal of Applied Mechanics 29, 109.